THE ASTROPHYSICAL JOURNAL, 196:381–405, 1975 March 1

DENSITY WAVE THEORY AND THE CLASSIFICATION OF SPIRAL GALAXIES

WILLIAM W. ROBERTS, JR.*
University of Virginia
MORTON S. ROBERTS
National Radio Astronomy Observatory†
AND
FRANK H. SHU‡
University of California at Berkeley
Received 1974 June 27; revised 1974 September 20

ABSTRACT

Axisymmetric models of disk galaxies taken together with the density wave theory allow us to distinguish and categorize spiral galaxies by means of two fundamental galactic parameters: the total mass of the galaxy, divided by a characteristic dimension; and the degree of concentration of mass toward the galactic center. These two parameters govern the strength of the galactic shocks in the interstellar gas and the geometry of the spiral wave pattern. In turn, the shock strength and the theoretical pitch angle of the spiral arms play a major role in determining the degree of development of spiral structure in a galaxy and its Hubble type. The application of these results to 24 external galaxies demonstrates that the categorization of galaxies according to this theoretical framework correlates well with the accepted classification of these galaxies within the observed sequences of luminosity class and Hubble type.

Subject headings: galactic structure — galaxies — shock waves — star formation

I. INTRODUCTION

From his extensive studies of the morphology of galaxies, Reynolds (1927) suggested a refinement to Hubble's (1926) classification which would take into account the bulkiness of the arms of spiral galaxies of similar Hubble type. He uses the terminology of "filamentary" and "massive" to distinguish the extremes. Examples are M101 (NGC 5457) for the former and M33 (NGC 598) for the latter type; both are Sc's in the Hubble system. This suggestion went essentially unnoticed in later discussions of the apparent structure of spirals (but see Hubble 1936, p. 44) until van den Bergh (1960*a*, *b*) found a correlation between the intrinsic luminosity of a spiral galaxy and the "degree to which spiral structure is developed...." Using criteria similar to Reynolds's "filamentary" and "massive" arms (and including the surface brightness), van den Bergh assigned luminosity classes to many of the galaxies in the Shapley–Ames (1932) catalog on the basis of their photographic image on the Palomar Sky Survey prints. The notation he adopts is similar to that used in stellar spectral classification: the roman numeral I denotes the intrinsically bright spiral galaxies with well-developed, "filamentary" spiral arms; and successive roman numerals denote intrinsically fainter spiral galaxies with less well-developed, "massive" spiral arms. His class V corresponds to a "dwarf" spiral some 4 mag fainter than class I. In his notation the two examples noted above are Sc I for M101 and Sc II–III for M33.

Any complete theory of spiral structure must be able to account for this remarkable variety in a natural way. A viable candidate at the present time is the density wave theory (see the review by Lin 1971) which addresses itself primarily to the dilemma of the persistence of spiral structure in a field of differential rotation and to the mechanism of formation of the stars which delineate spiral arms. In this theory, the enhanced luminosity of a spiral arm is believed to originate in the very young, newly formed stars whose births from interstellar clouds have been triggered by the passage of the crest of a spiral density wave. One wonders if this same wave mechanism can also account for the ordering of spirals into luminosity class and Hubble type. This is the issue which motivates the present work.

Within the context of the density wave theory, we show that a categorization of disk-shaped galaxies with spiral structure is possible by means of two fundamental parameters. These two parameters are: the total mass divided by the characteristic dimension of the galaxy, and the degree of concentration of mass toward the galactic center. The latter determines the pitch angle i of the spiral arms; and taken together, the two parameters determine $w_{\perp 0}$, the velocity component of basic rotation normal to the spiral arms. It is $w_{\perp 0}$ which so strongly influences the strength of the galactic shock wave. These results are applied to 24 extragalactic systems, and clear correlations between these theoretical quantities and the observed sequences of luminosity class and Hubble type are found.

* On sabbatical leave at the Kapteyn Institute, University of Groningen, The Netherlands.

† Operated by Associated Universities, Inc., under contract with the National Science Foundation.

‡ Alfred P. Sloan Foundation Fellow, 1972–1974.

II. THE CONSTRUCTION OF GALACTIC MODELS

We model a spiral galaxy to consist of two components, gas and stars, which are in gravitational interaction with one another. In disk galaxies, the gas is known to be concentrated in a very thin layer whose thickness is only a few percent of the diameter of the disk. Until recently, it was commonly accepted that the major portion of the mass of the stellar component is also confined to a fairly thin disk; however, recent work on the susceptibility of such configurations to barlike instabilities (see esp. Ostriker and Peebles 1973) has raised the possibility that spiral galaxies might have very massive halos.

In our work, we have retained the conventional view that most of the mass is distributed in a disk plus a central bulge. The inclusion of a stellar halo with mass comparable to that of the disk would influence our main results only in an indirect way since a more or less spheroidal halo exerts no direct influence on the dynamics of the spiral structure in the disk. However, its presence would affect the basic surface density σ_0 which one would deduce to be present in the disk on the basis of an examination of the *observed* rotation curve inasmuch as only a fraction of the source of the axisymmetric gravitational field would then be associated with the distribution of mass in the disk. The net effect would be to lower the length scale, $k_T^{-1} = 2\pi G\sigma_0/\kappa^2$, (Toomre 1964) which characterizes the collective gravitational interactions of a differentially rotating disk whose local epicyclic frequency is κ. Since the radial spacing of consecutive spiral arms would then be lowered proportionally, it would be necessary, in order to obtain the *same* fit for an observed spiral pattern, to raise either the pattern speed Ω_p or the stability parameter Q (see also § VI) or both. We have not felt such a course of action to be warranted at the present state of our knowledge of the role of stellar halos. In any case, since this correction would need to be applied to every galaxy in our sample, the main trends (§§ IV and V) revealed by our analysis would probably remain unchanged.

a) Mass Models

Various kinds of self-consistent axisymmetric mass models have been considered for the stellar populations of galaxies based upon their observed rotation curves (Schmidt 1956, 1965; Burbidge, Burbidge, and Prendergast 1959; Brandt 1960; Toomre 1963; Freeman 1970). In the present investigation, an overall mass model is taken to consist of a flattened disk (Toomre 1963) to represent the disk population, and a superposition of one or two inhomogeneous spheroids to cover the central bulge, where necessary. Our procedure follows that described by Shu, Stachnik, and Yost (1971) except that it has been standardized and automated to provide the best least-squares fit to the rotation curve data. In particular, this procedure automatically selects the number of spheroidal components (zero, one, or two) to be superposed on the Toomre component, as well as providing the best values for the length scales A and angular velocity scales B, once the model numbers (n_T and n_S) and eccentricities (e_S) of the various components have been chosen.

For each model component, the model number is a measure of the relative degree of central concentration. For example, the flat Toomre component always plays the most important role, and the radius, $\varpi_{0.5M}$, at which half its mass lies inside and half outside, can be found to be

$$\varpi_{0.5M} = A_T(2^{2/(2n+1)} - 1)^{1/2}, \qquad (1)$$

where $n = n_T - 1$, and n_T is the Toomre model number. We shall find the half-mass radius, $\varpi_{0.5M}$, to be a useful concept, and we shall generalize its definition to include a superposition of component models. (The formula relating $\varpi_{0.5M}$ to the A's and B's is then no longer so simple as eq. [1].)

Figure 1 shows the rotation velocity data for the sample galaxy, NGC 157.[1] Superposed is the rotation curve corresponding to the mass model that provides the best least-squares fit to the rotation velocity data for each of several values of the model number, n_T. NGC 157 is one sample galaxy in which no spheroidal components are found to be necessary, and the Toomre component alone is sufficient. This galaxy is typical of most of the galaxies to be considered in § IV in the sense that the H II regions, constituting the rotation velocity data, and the visible spiral structure extend from the inner regions to the edge of the "easily visible" disk,[2] which itself generally lies well within the Holmberg radius.[3] In this galaxy as well as in many of the others, the rotation velocity data appear to reach a peak very close to the outermost data point, and this in turn lends uncertainty to the exact location of the real peak and to the value of n_T that allows for the best fit. However, it is important to note that the rotation curves for all these models spanning a large range of n_T values are all rather similar, particularly inside the region covering the "easily visible" disk where the spiral structure is prominent. For this reason the results herein do not depend in a sensitive manner on the choice of n_T. Therefore, a typical value of 5 is adopted for n_T in the Toomre component here as well as for n_S in each spheroidal component necessary for other galaxies considered in § IV.[4]

b) Velocity Dispersions

Following Shu *et al.* (1971), the overall mass model is adopted to have a finite but small disk thickness with a Schwarzschild distribution of peculiar velocities at each point. In this approach the velocity dispersion in the radial direction, $\langle c_\varpi^2\rangle^{1/2}$, and the velocity dispersion in the vertical direction, $\langle c_z^2\rangle^{1/2}$, can be arbitrarily specified. With regard to the ratio, $\langle c_z^2\rangle^{1/2}/$

[1] Rotation velocity data for NGC 157 and the estimate of its distance of 24.0 Mpc, based on a Hubble constant of $H = 75$, are taken from Burbidge *et al.* (1961*b*).

[2] "Easily visible" refers to eye estimates made by the authors.

[3] The Holmberg radius is based on the angular measurements of Holmberg (1958).

[4] The entire sequence of values for n_T is also considered later in §§ IV and VI.

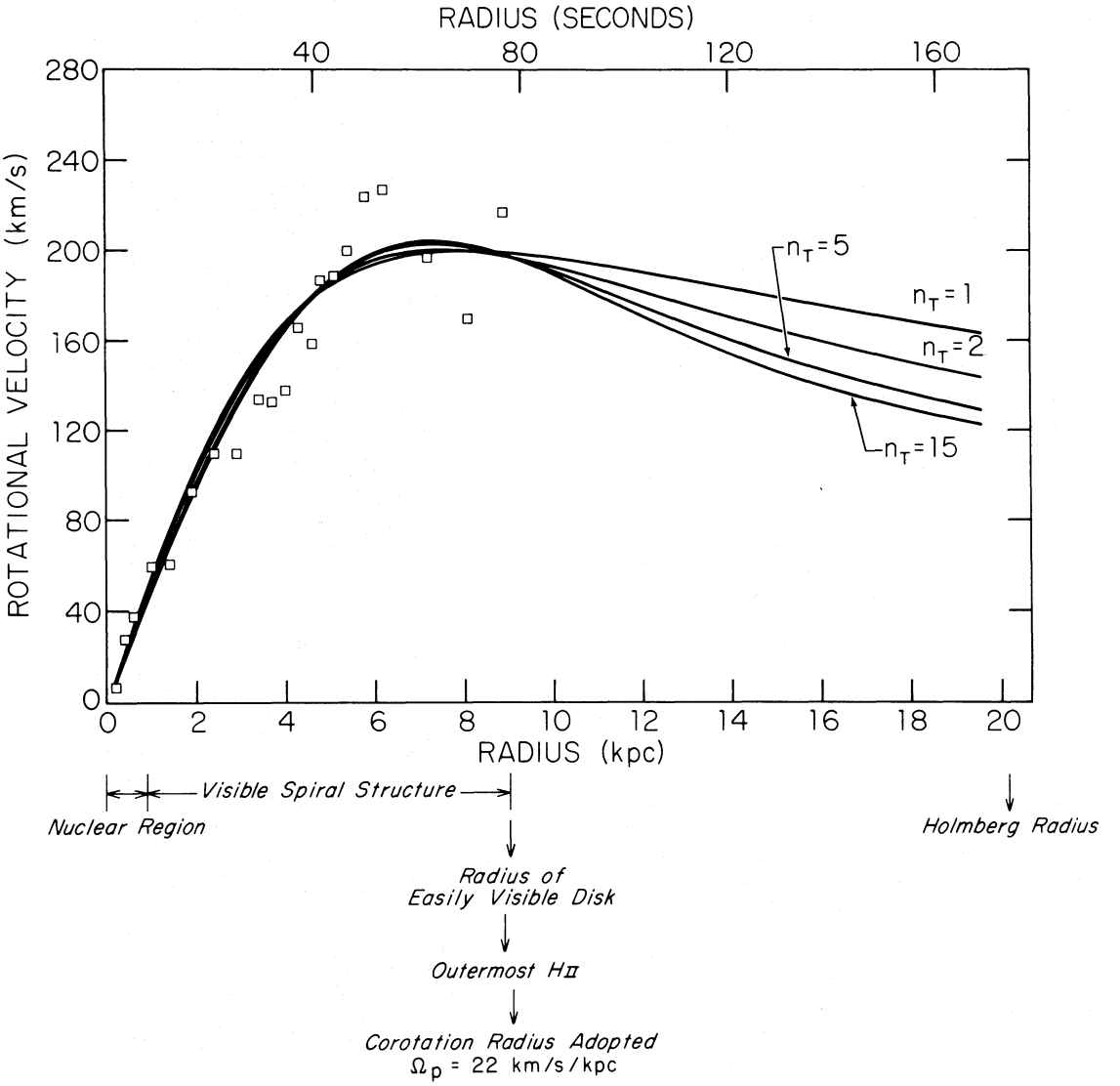

FIG. 1.—Rotation velocity data for the sample galaxy NGC 157, derived from H II regions, □, observed by Burbidge *et al.* 1961*b*. Superposed is the rotation curve corresponding to the mass model for the equilibrium disk which provides the best least-squares fit to the rotation velocity data for each of several values of the model number, n_T (no spheroidal components are necessary). The radial extent of the observed distribution of H II regions coincides with the radial extent of the visible spiral structure and the edge of the "easily visible" disk. Over the radial extent of these three tracers of spiral structure and recent star formation, the rotation curve is relatively insensitive to n_T.

$\langle c_w^2 \rangle^{1/2}$, Shu *et al.* suggest that it should have a value near unity in the central regions where a well-mixed state of equilibrium might be expected to prevail, and it probably reaches a value substantially less than unity in the outer regions where the motions perpendicular to the galactic plane are substantially decoupled from those parallel to it. For definiteness, we thus adopt the following relation:

$$\langle c_z^2 \rangle^{1/2} / \langle c_w^2 \rangle^{1/2} = 1.0 - 0.5(\varpi/\varpi_{\rm edge}) , \qquad (2)$$

where $\varpi_{\rm edge}$ is taken to correspond to the observed Holmberg radius of the galaxy.

To determine $\langle c_w^2 \rangle^{1/2}$, we specify it as a ratio of the actual radial velocity dispersion to the minimum required to suppress all axisymmetric gravitational instabilities, $Q = \langle c_w^2 \rangle^{1/2} / \langle c_w^2 \rangle_{\rm min}^{1/2}$. Toomre (1964) showed how $\langle c_w^2 \rangle_{\rm min}^{1/2}$ could be determined for a stellar disk of infinitesimal thickness, and Shu *et al.* (1971) summarized the generalization given by Shu (1968) and Vandervoort (1970) for stellar disks of finite thickness. The results applied to the solar neighborhood show Q to be close to unity, but it may be substantially larger in the central regions of the Galaxy if the barlike instability is to be suppressed (see, e.g., Kalnajs 1972; also Toomre 1974; Wielen 1974). On the other hand, if we allow ourselves the freedom to vary Q arbitrarily with ϖ, we could fit almost any observed spiral pattern with arbitrary accuracy. To eliminate this degree of freedom, we

adopt in this paper the hypothesis

$$Q = 1.0 \qquad (3)$$

throughout the disk. We have examined the effect of varying Q and have found that better fits can often be obtained by allowing Q to be somewhat larger than unity in the inner portions of a galaxy where our computed spiral patterns tend sometimes to be too tightly wound. However, the determination of Q is such a vexing question, both theoretically and observationally, that it would be well beyond the scope of the present paper to settle the issue here. We merely remark that by adopting hypothesis (3), our fits for the spiral pattern contain only one free parameter, the pattern speed Ω_p (or, equivalently, ϖ_c, the radius where the matter corotates with the spiral wave).

c) *Corotation Radius of Spiral Density Waves*

With an equilibrium model of the type just discussed, the theoretical pattern of density waves in the stellar disk can be computed from the known dispersion relationship once an estimate of the pattern speed Ω_p is made. The radius where corotation occurs, and consequently the speed Ω_p at which the pattern rotates, are expected to influence the radial extents of at least three easily observable tracers: (1) the prominent spiral structure, (2) the "easily visible" disk, and (3) the distribution of H II regions in the original rotation curve study. In this paper the pattern speed Ω_p is adopted so that the radius of corotation, ϖ_c, lies nearly coincident with the radial extents of all three tracers, or with some representative median when the tracers differ substantially in extent (as indicated in tables 1 and 2). For NGC 157, shown in figure 1, the radial extents of these three tracers of spiral structure and recent and current star formation are about the same, and a natural choice for the corotation radius is one coincident with the edges of all three. This criterion to estimate corotation is the standard applied in § IV to each of the 24 external galaxies.

d) *Shock Waves in the Interstellar Gas*

Galactic shock waves are found to form in the gaseous component of a galaxy as a necessary consequence of the theory for forced spiral waves of sufficiently large amplitude (W. W. Roberts 1969; Shu, Milione, and Roberts 1973; Woodward 1973). In our view galactic shocks provide the triggering mechanism for the gravitational collapse of gas clouds, eventually leading to the formation of stars along a spiral arm. For a given wave amplitude, the *strength of the shock and the degree of compression of the gas vary as the square of the ratio*, $w_\perp/a$, where $w_\perp$ is the total (unperturbed plus perturbed) velocity component of the gas normal to a spiral arm and a is the effective acoustic speed of the interstellar gas. If the two-component model of the interstellar medium is adopted, a is unlikely to be very different from the sound speed associated with the intercloud medium, 7–12 km s^{-1}, and a mean value of a in this range might be dictated by the atomic physics of all spiral galaxies.

On the other hand, $w_\perp$ oscillates along a streamline about its unperturbed value $w_{\perp 0}$ because of the forcing of the spiral gravitational field of fractional amplitude, F. Shocks form if F is sufficiently large to force $w_\perp$ to achieve transonic values. For $w_{\perp 0} > a$, most of the gas on the streamline is moving at supersonic speeds while only a small portion is moving subsonically. The shocks that form in this situation tend to be *strong* and give rise to *narrow* regions of *high* gas compression. For $w_{\perp 0} < a$, most of the gas on the streamline is moving subsonically while only a small portion travels supersonically. In this situation the shocks tend to be *weak* and yield rather *broad* regions of relatively *low* gas compression (Shu *et al.* 1973). Therefore, the strength of the shock and compression of the gas and the consequent theoretical differentiation between spiral structure with *narrow* "filamentary" arms and *broad* "massive" arms seem to be critically dependent on the quantity

$$w_{\perp 0} = \varpi(\Omega - \Omega_p) \sin i\,, \qquad (4)$$

where i is the pitch angle of the wave pattern which is to be obtained from the dispersion relationship once Ω_p is given.

Figure 2 shows the theoretical curves of $w_{\perp 0}$, i, and F in the sample galaxy NGC 157 for several different choices of the pattern speed Ω_p. The two-headed arrows indicate the range of radii for which the asymptotic calculations are considered numerically reliable (in accordance with the criteria adopted by Shu *et al.* 1971). The corresponding curves of each set appear to be rather similar and are relatively insensitive to the choice of pattern speed. Each of the curves of $w_{\perp 0}$, for example, attains a peak of moderate to large magnitude in the range of 15–20 km s^{-1}, and this indicates that moderately strong shocks are possible. NGC 157 is therefore one sample galaxy in which moderately well developed spiral structure would be predicted to be possible. The value of $w_{\perp 0}$ at about one-half the corotation radius appears to be a rather typical value representative of the magnitude of $w_{\perp 0}$ over a substantial portion of the "easily visible" disk, and for future comparison of a number of galaxies with one another this value of $w_{\perp 0}$ at one-half corotation in each galaxy is frequently used. Fortunately, the quantity $w_{\perp 0}$ is independent of the assumed distance, and therefore any uncertainty stemming from the estimates of distances of various galaxies will not enter here. Partly for this reason and partly for the reason that $w_{\perp 0}$ is relatively insensitive to the choice of corotation radius, $w_{\perp 0}$ will be one of the most important parameters to be used in comparing various galaxies in later sections.

Contained in figure 3 is a photograph of the sample galaxy NGC 157 with its moderately well developed spiral arms taken from the Hubble Atlas (Sandage 1961). The moderately well developed spiral structure is thought to be a consequence of the moderately strong shocks possible in this galaxy. For the purpose

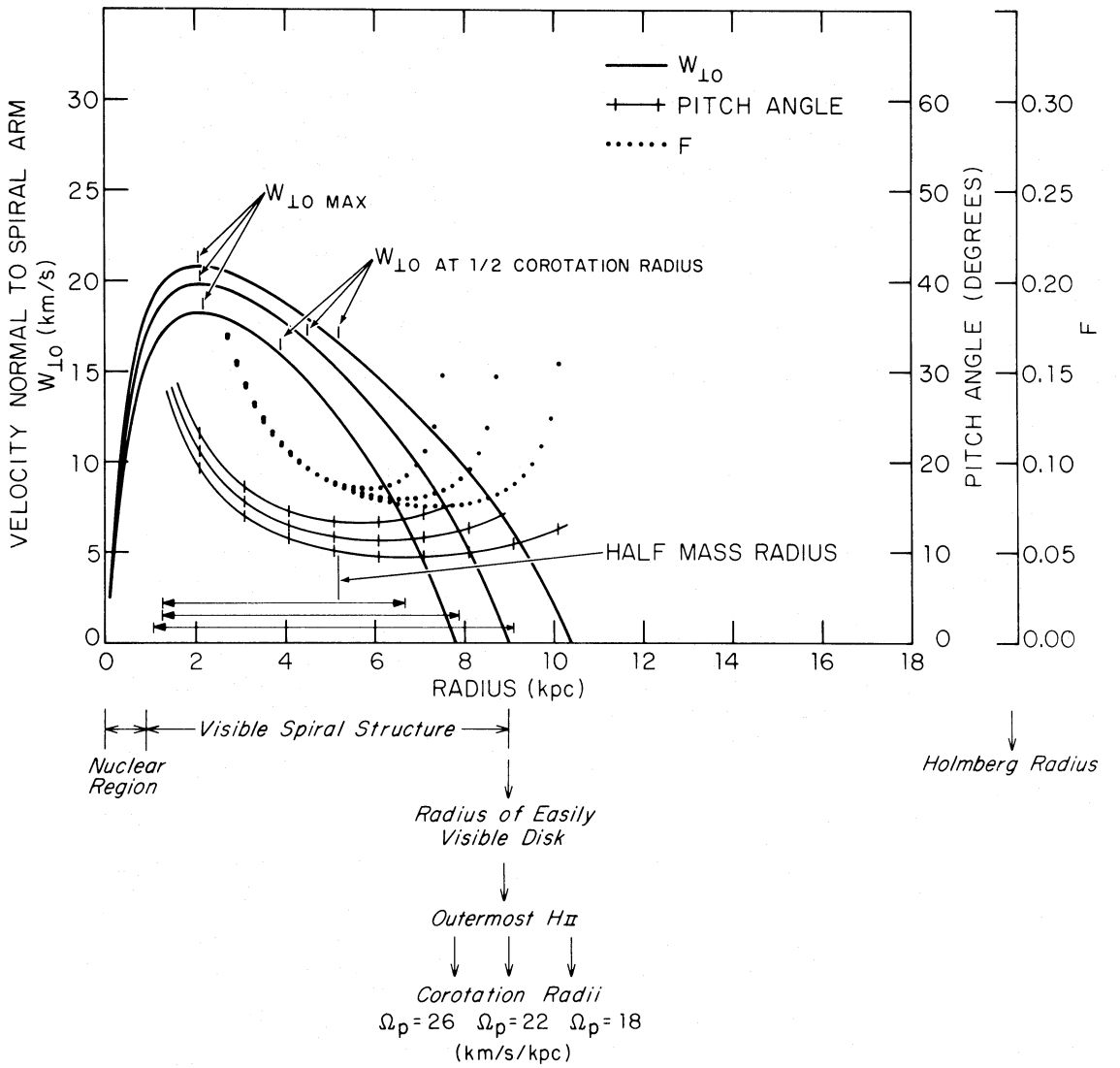

FIG. 2.—Characteristics of the wave pattern in the density wave model of the sample galaxy NGC 157. The quantity $w_{\perp 0}$ measures the velocity component of basic rotation normal to a spiral arm; i, the theoretical pitch angle of the same wave arm; and F, the ratio of the magnitude of the spiral gravitational field of the wave pattern to that of the central axisymmetric field. To show their dependence on the pattern speed, $w_{\perp 0}$, i, and F are sketched for each of three values of pattern speed Ω_p. The corresponding curves of the three sets are all rather similar and actually rather insensitive to the value of Ω_p. The galactic shock wave is viewed as a possible triggering mechanism for star formation along a spiral arm, and the strength of the shock can be estimated by the square of $w_{\perp 0}$. Since $w_{\perp 0}$ attains a substantial level for all cases in the range, 15–20 km s^{-1}, over a large region of the disk, moderately strong shocks are possible; and NGC 157 is capable of exhibiting moderately well-developed spiral structure over its disk.

of illustrating the sensitivity of the theoretical pattern to choice of pattern speed, this photograph has superposed on it the theoretical patterns calculated for two of the possible choices of pattern speed, $\Omega_p = 22$ and 26 km s^{-1} kpc^{-1}, illustrated in figure 2. Each pattern is sketched over a radial extent equivalent to its range of validity. Both patterns coincide well with the observed spiral structure; however, the more extensive pattern for $\Omega_p = 22$ km s^{-1} kpc^{-1} seems to satisfy better the criterion for corotation and to cover the radial extents of the prominent spiral structure and "easily visible" disk (and distribution of H II regions) a little more completely. For this reason, this pattern with corotation at 9 kpc is adopted for NGC 157. Since it is sketched only over its range of validity, 1.2–7.8 kpc, the adopted pattern is somewhat more extensive than the sketch might appear to indicate. Corotation at 9 kpc therefore lies about 15 percent farther out in the disk than the outermost point of the sketch at 7.8 kpc.[5]

[5] The theoretical behavior of spiral density waves near corotation is more complicated, even in the linear regime, than has been previously assumed. Mark (1974*b*; see also in Lin 1970, Feldman and Lin 1973) has shown that the trailing free-wave configuration near corotation cannot be represented as a single continuous wave, but must comprise three waves—

III. THEORETICAL CATEGORIZATION OF SPIRAL GALAXIES

In the preceding section the synthesis of axisymmetric models of disk galaxies with the density wave theory provides the theoretical framework for a deeper understanding of the important quantities $w_{\perp 0}/a$ and i, which are suggested to characterize wave phenomena among spiral galaxies. The quantity $w_{\perp 0}/a$ measures the tendency for the production of *strong* shocks with *narrow* regions of *high* gas compression. However, since we have already reasoned that a may have very similar values for all spiral galaxies, we will thus regard $w_{\perp 0}$ and i as the two important quantities which characterize wave phenomena in spiral galaxies. Dimensional analysis shows that typical values of $w_{\perp 0}$ and i (say, at half the corotation radius) can be expressed as

$$w_{\perp 0} = (GM/\varpi_c)^{1/2} f(\varpi_{0.5M}/\varpi_c)\,, \tag{5a}$$

$$\sin i = g(\varpi_{0.5M}/\varpi_c)\,, \tag{5b}$$

where f and g are functions whose forms are specified once the equilibrium disk has been specified except for scale factors. In equation (5a), G is the universal gravitational constant and M is the total mass of the galaxy. The combination GM/ϖ_c is a measure of the potential energy divided by the mass of the galaxy. Thus, we arrive at the fundamental conclusion of this paper: *The two critical and fundamental parameters which underlie the determination of the characteristics and the geometric form of normal spirals are* M/ϖ_c (*or, equivalently,* $M/\varpi_{0.5M}$) *and* $\varpi_{0.5M}/\varpi_c$.[6] In §§ IV and V we shall show that the categorization of galaxies by these two parameters correlates well with the accepted classification of galaxies within the observed sequences of luminosity class and Hubble type.

Figure 4 illustrates a practical application of these ideas. Plotted on the vertical axis is $w_{\perp 0}$ evaluated at half-corotation for an ensemble of hypothetical galaxies whose basic mass distribution is given by Toomre's model 5. The corresponding surface generated by computing $w_{\perp 0}$ for different values of $M/\varpi_{0.5M}$ and $\varpi_{0.5M}/\varpi_c$ will be referred to as the $w_{\perp 0}$ surface. In this figure, it has been calculated by considering a grid at equal intervals of $M/\varpi_{0.5M}$ and $(\varpi_{0.5M}/\varpi_c)^{-1}$.

The value of $w_{\perp 0}(0.5\varpi_c)$ for a given galaxy with specified mass M and specified half-mass radius $\varpi_{0.5M}$ can be determined along this surface for each of several different choices of the galaxy's pattern speed. The sequence of locations will follow a given curve of constant $M/\varpi_{0.5M}$. As an example, the black dots indicate the values of $w_{\perp 0}(0.5\varpi_c)$ for the sample galaxy NGC 157 for six different pattern speeds (so indicated in parentheses). For Ω_p small, the radius at half corotation is near inner Lindblad resonance and the value of $w_{\perp 0}$ is small. As Ω_p is increased, ϖ_c decreases and both $\varpi_{0.5M}/\varpi_c$ and i increase. At first, $w_{\perp 0}$ increases with sin i until a maximum is reached on the ridge of the $w_{\perp 0}$ surface. Here the rate of decrease of $(\Omega - \Omega_p)\varpi$ overtakes the rate of increase of sin i as Ω_p is further increased, and $w_{\perp 0}$ decreases slowly thereafter with increasing Ω_p and $\varpi_{0.5M}/\varpi_c$. All six cases of pattern speed are sketched here for the purpose of illustration only, since the criterion adopted for determining corotation has already been applied to NGC 157 in the previous section to yield the selection of $\Omega_p = 22$ km s^{-1} kpc^{-1} as the best estimate. For NGC 157, as for all galaxies to be considered later, $\varpi_{\rm edge}$ is taken as the observed Holmberg radius. On the other hand, the ensemble spanning the surface consists of cases in which $\varpi_{\rm edge}$ is taken as the typical scale A_T for each case. For this reason, NGC 157 is actually displaced slightly from the surface in several of the cases (as indicated by the very short vertical lines above several of the black dots). The three coordinates in this representation are ideal in the sense that they are distance-independent parameters, and any uncertainty that may be present in the estimate of distance of a galaxy does not enter here.

IV. RESULTS FOR TWENTY-FOUR EXTERNAL GALAXIES AND OUR OWN GALAXY

From the sample of galaxies with published rotation curves (except those for the Magellanic Clouds), 24 galaxies are selected on the basis of the following criteria: (1) The galaxy has a luminosity class assigned by van den Bergh (1960*a*, *b*) and, (2) the rotation curve extends, and is complete in its coverage, over a significant fraction of the photometric radius of the galaxy. When more than one rotation curve is available, the one chosen is indicated in the references to table 1. Specific comments regarding the radial velocity data for individual galaxies are noted in the Remarks column in table 1. Other entries in this table include van den Bergh's (1960*a*, *b*) type classification (col. [2]), and luminosity class (col. [3]). Because these type classifications are based on the small scale (and often dense images) of the Palomar Sky Survey, column (4) is added to give the classifications of the *Reference Catalogue of Bright Galaxies* (de Vaucouleurs 1964). With two exceptions, NGC 972 and NGC 3593, these two type classifications agree to within one class; most, to within half a class. The adopted distance, column (5), and inclination, angle between the principal plane of the galaxy and the plane of the sky, column (6), are taken from the original reference for the rotation curve data, column (10): Burbidge and Burbidge (BB); Burbidge *et al.* (1964) (BBCRP); Burbidge, Burbidge, and Prendergast (BBP); van Damme (1966) (van D); Demoulin (1969) (D); Fish (1961) (F); Gordon (1971)

two short waves which propagate radially in opposite directions and one long wave which propagates from the interior. Our modelings do not attempt to incorporate these effects, nor do they attempt to give an accurate representation of the behavior near the Lindblad resonance along the lines developed by Mark (1974*a*). Thus, our sketches of the spiral patterns show only the ranges of radii where the inwardly propagating short waves are expected to predominate in their usual simple form.

[6] Ostriker and Peebles (1973) point out that the dimensionless quantity, the ratio of a galaxy's rotational kinetic energy and its gravitational potential energy, determines its basic shape (i.e., flatness). This third dimensionless parameter plays no role in our work because we restrict our attention to galaxies of one basic shape, namely, disk galaxies.

1975ApJ...196..381R

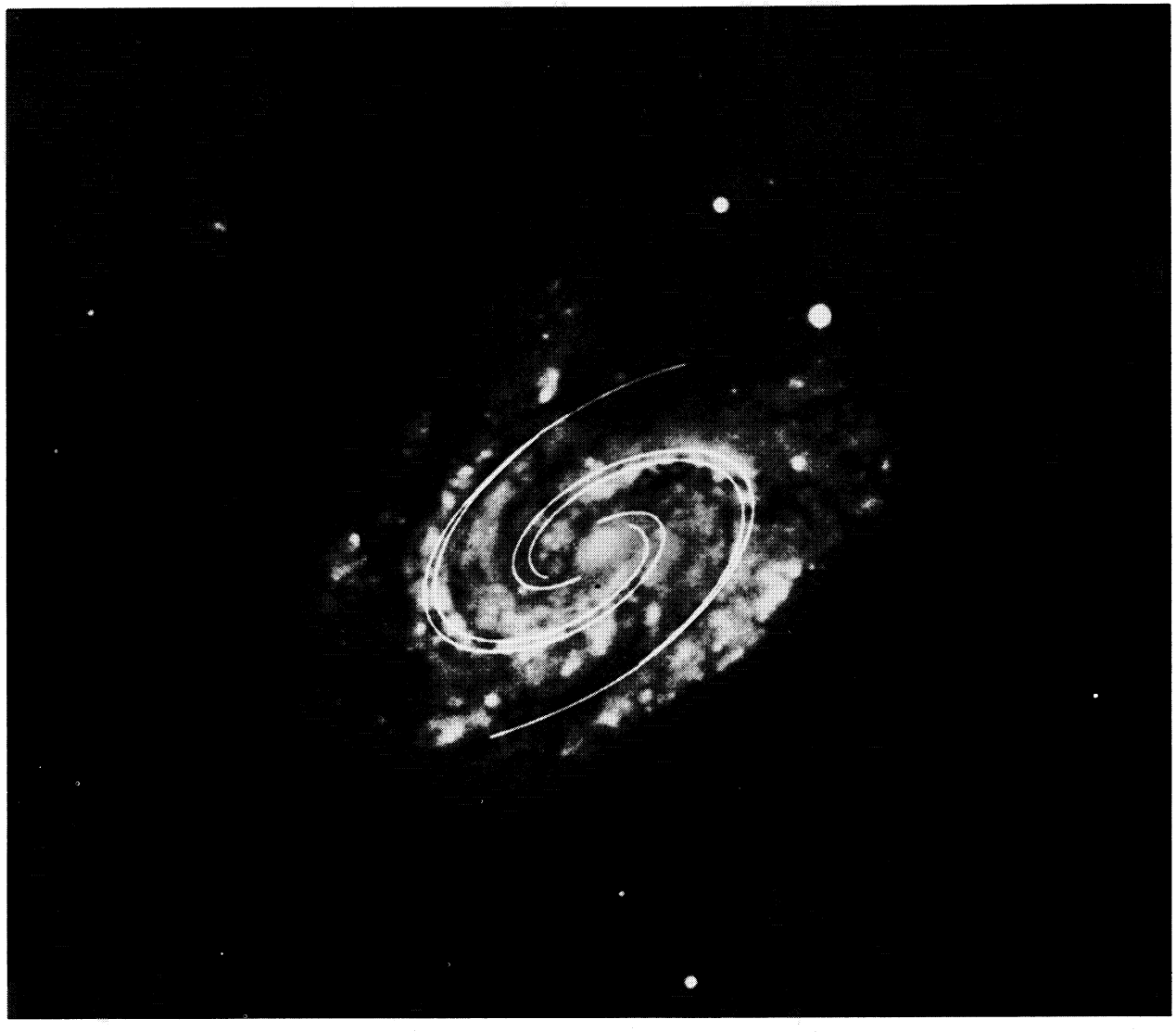

FIG. 3.—Photograph of the sample galaxy NGC 157 with its moderately well developed spiral arms taken from the Hubble Atlas. The wave patterns for two values of the pattern speed Ω_p (22 and 26 km s^{-1} kpc^{-1}) are superposed to illustrate the sensitivity to Ω_p. The more extensive pattern for $\Omega_p = 22$ km s^{-1} kpc^{-1} is adopted since it better satisfies the criterion for corotation and covers more adequately the radial extent of the observed spiral structure and "easily visible" disk. This pattern is sketched only over its range of validity, 1.2–7.8 kpc, and corotation at 9 kpc actually lies about 15% farther out in the disk from the edge of the sketch (at 7.8 kpc).

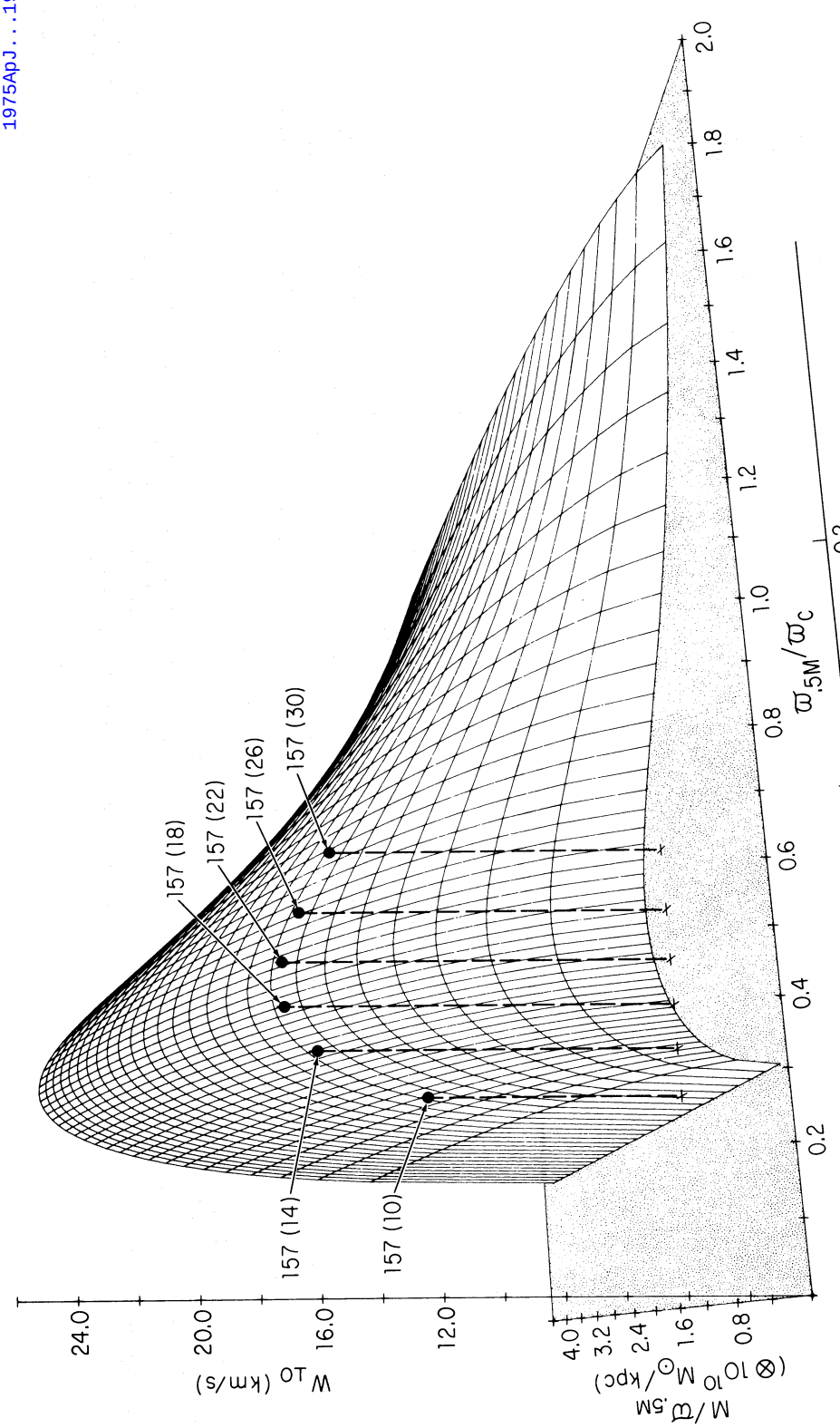

FIG. 4.—Theoretical categorization of disk-shaped galaxies; a representation of an ensemble of cases, spanning the two dimensional parameter space: $M/\varpi_{0.5M}$, $\varpi_{0.5M}/\varpi_c$. The mass model simulating the equilibrium state for each case in the ensemble is one of Toomre type, with no spheroidal components superposed, and ϖ_{edge} is taken as the typical scale A_T for each case. The quantity $w_{\perp 0}$ is evaluated at half-corotation for all cases, and the $w_{\perp 0}$ surface so generated is a measure of the strength of the galactic shock possible over this ensemble. The sample galaxy NGC 157 is sketched in this representation for each of six different values of pattern speed to illustrate how the values for $w_{\perp 0}$ at half-corotation in a given galaxy might vary over this surface with Ω_p. For reasonable values within the earlier adopted neighborhood of $\Omega_p = 22$ km s^{-1} kpc^{-1}, the variation of $w_{\perp 0}$ is not great.

1975ApJ...196..381R

TABLE 1

OBSERVATIONAL DATA

NGC (1)	Type (van den Bergh) (2)	Luminosity Class (van den Bergh) (3)	Type (de Vaucouleurs) (4)	Distance (Mpc) (5)	Inclination (degrees) (6)	Radius of Easily Visible Disk (kpc) (7)	Radius of Outermost H II Region (kpc) (8)	Holmberg Radius (kpc) (9)	References (10)	Remarks (11)
157.....	Sc(*)	I	SAB(rs)bc	24.0	58.6	9.0	8.9	20.2	BBP 1961*b*	
224.....	Sb	I–II	SA(s)b	0.69	77.0	13.0	22.5	19.8	RF 1970	
598.....	Sc	II–III	SA(s)cd	0.72	55.0	4.8	5.2	8.7	G 1971, RS 1972	
925.....	S(B)c	II–III	SAB(s)d	6.8	53.0	7.7	9.0	13.8	RBB 1964, RRW 1967	7
972.....	Sc(n)	II:	I0	22.1	66.3	4.7	4.0	(15.4)	BBP 1965	1
1084.....	Sc	I–II	SA(s)c	19.2	65.0	5.2	5.2	(12.9)	BBP 1963	1
1832.....	Sc	II	SB(r)bc	25.3	60.0	6.0	6.1	(16.2)	BB 1968	1
2403.....	Sc	III	SAB(s)cd	3.25	60.0	4.6	6.7	13.7	RS 1972	
2903.....	Sb$^+$	I–II	SAB(rs)bc	7.9	70.0	12.6	5.3	16.1	BBP 1960*b*	3
3031.....	Sb	I–II	SA(s)ab	3.2	55.0	8.9	16.2	16.3	M 1959	
3109.....	Ir$^-$	IV–V	Im sp	2.2	90.0	6.0	3.1	(5.9)	van D 1966	1
3389.....	Sc*	III:	SA(s)c	15.0	62.0	3.2	2.6	(8.7)	RF 1967	1
3521.....	Sb$^+$	II	SAB(rs)bc	8.5	65.5	6.2	7.3	16.8	BBCRP 1964	
3593.....	Sb	III	SA(s)0/a:	7.0	75.0	1.2	4.1	(7.0)	D 1969	1
4236.....	SB$^+$ or Ir$^+$	IV	SB(s)dm	3.25	75.0	9.6	...	12.3	S 1973	
4631.....	Sc*	III?	SB(s)dsp	4.4	85.0	7.3	7.0	12.2	de V, de V 1963	
5005.....	Sb$^-$	II	SAB(rs)bc	14.4	66.0	8.0	5.7	16.8	BBP 1961*a*	
5055.....	Sb$^+$	II	SA(rs)bc	7.3	58.6	6.5	7.3	17.0	BBP 1960*a*, F 1961	
5194.....	Sc(t)	I	SA(s)bcp	4.0	35.0	5.0	5.5	8.3	BB 1964, T 1972	6
5457.....	Sc	I	SAB(rs)cd	6.9	22.0	15.5	15.3	28.1	RS 1972	
6946.....	Sc	I (or II)	SAB(rs)cd	10.1	30.0	12.3	11.9	(27.9)	RS 1972	2
7331.....	Sb	I–II	SA(s)bc	14.4	69.1	18.4	(10.4)	28.5	RBBCP 1965	4
7479.....	SBb$^+$	I	SB(s)c	35.2	44.5	15.6	(11.6)	(31.3)	BBP 1960*c*	1, 5
IC342.....	Sc	I	SAB(rs)cd	4.5	25.0	11.0	...	(26.1)	RS 1972	2

REMARKS TO TABLE 1

1. Holmberg radius from M. S. Roberts (1969), eq. (2).
2. Holmberg radius from Rogstad and Shostak (1972).
3. Corotation radius adopted as radius of outermost H II region.
4. Five outermost velocity data points are assigned low weight and are not used in the determination of the rotation curve because of their large scatter. Upon exclusion of these five H II regions, the next outermost H II region at 10.4 kpc is adopted as the corotation radius.
5. Four outermost velocity data points are assigned low weight and are not used in the determination of the rotation curve because of their large scatter. The radius of the "easily visible" disk is adopted as the corotation radius.
6. Two sources of velocity data are considered from the published literature. First, the velocity data from Burbidge and Burbidge (1964) is adopted to determine a rotation curve; and a corresponding density wave pattern is computed with $\Omega_p = 42$ km s^{-1} kpc^{-1}. Second, the velocity data from Tully (1972) is adopted to determine a rotation curve; and a corresponding density wave pattern is computed with $\Omega_p = 90$ km s^{-1} kpc^{-1} (later referred to as 5194_T or 5194*).
7. To extend the range in radius, one data point at 7 kpc from 21-cm measurements by Rogstad *et al.* (1967) is added to the optically measured data.

TABLE 2

THEORETICAL RESULTS

NGC (1)	Components of Equilibrium Model: $n_T = 5$ (2)	$n_s = 5$, $e_s = 0.8661$ (3)	$n_s = 5$, $e_s = 0.9880$ (4)	Mass M ($\times 10^{10}\ M_\odot$) (5)	Half-Mass Radius $\varpi_{0.5M}$ (kpc) (6)	Pattern Speed Ω_p (km s^{-1} kpc^{-1}) (7)	Corotation Radius ϖ_c (kpc) (8)	Central Mass Concentration $\varpi_{0.5M}/\varpi_c$ (9)	Velocity $(\Omega-\Omega_p)\varpi$ (km s^{-1}) (10)	Pitch Angle i ($0.5\varpi_c$) (degrees) (11)	Velocity $w_{\perp 0}(0.5\varpi_c)$ (km s^{-1}) (12)
157.....	T			6.8	5.2	22.0	9.0	0.58	78.1	12.3	16.7
224.....	T	S	S	17.8	7.0	18.0	14.0	0.50	129.7	9.5	21.5
598.....	T	S		1.3	3.5	32.0	2.8	1.24	24.8	19.6	8.3
				(1.9)	(4.7)	(32.0)	(2.8)	(1.67)	(31.3)	(16.0)	(8.7)
925.....	T			1.8	4.9	14.0	7.7	0.64	35.1	14.4	8.7
972.....	T			1.0	1.8	29.0	4.0	0.46	67.1	8.8	10.2
1084.....	T	S		1.9	2.4	27.0	5.2	0.45	80.6	8.6	12.1
1832.....	T	S		4.1	3.2	31.0	6.0	0.53	86.4	10.5	15.7
2403.....	T	S		2.3	4.5	25.0	4.8	0.93	26.8	19.9	9.1
				(3.5)	(6.1)	(24.0)	(4.8)	(1.26)	(36.2)	(17.4)	(10.8)
2903.....	T			4.3	2.7	38.0	5.4	0.51	101.9	10.2	18.0
3031.....	T	S		12.5	5.5	26.0	9.7	0.57	103.1	11.8	21.0
3109.....	T			0.5	6.3	8.0	6.0	1.04	6.2	26.1	2.7
3389.....	T			2.2	2.3	65.0	2.6	0.87	31.6	20.8	11.2
3521.....	T	S		8.1	3.2	33.0	7.3	0.44	137.3	8.4	20.2
3593.....	T	S		0.2	0.4	80.0	1.2	0.37	73.7	5.4	6.9
4236.....	T	S		1.7	6.9	9.0	9.6	0.72	25.1	16.0	6.9
4631.....	T	S		2.5	6.2	15.0	7.3	0.84	23.1	19.9	7.9
5005.....	T	S		7.3	2.4	27.0	8.0	0.31	180.8	3.9	12.2
5055.....	T	S		5.8	2.1	32.0	6.6	0.31	177.6	4.0	12.4
5194*.....	T	S		3.3	2.6	42.0	4.5	0.58	77.7	11.7	15.7
				[2.4]	[1.2]	[90.0]	[2.4]	[0.51]	[106.9]	[9.6]	[17.9]
5457.....	T	S		14.5	10.9	13.0	15.5	0.70	58.9	15.7	15.9
				(19.4)	(13.5)	(13.0)	(15.5)	(0.87)	(58.0)	(16.8)	(16.7)
6946.....	T	S		11.5	8.1	17.0	12.3	0.66	68.4	14.2	16.7
				(19.7)	(12.0)	(16.0)	(12.3)	(0.98)	(74.8)	(14.2)	(18.3)
7331.....	T	S		7.8	3.4	19.0	10.4	0.32	152.3	4.9	13.0
7479.....	T			10.5	9.0	12.0	15.6	0.58	73.3	12.4	15.8
IC342.....	T	S		8.8	7.0	15.0	12.5	0.56	78.5	11.6	15.8
				(16.0)	(11.3)	(15.0)	(12.5)	(0.90)	(71.3)	(13.8)	(17.0)
Our Galaxy..	T	S		13.1	6.0	13.5	15.7	0.38	148.1	6.9	17.7

* Two extensive and independent rotation curve studies are available for this galaxy, NGC 5194. These are treated separately here. The first is from Burbidge and Burbidge (1964); the second is from Tully (1972).

(G); Münch (1959) (M); Rogstad, Rougoor, and Whiteoak (RRW); Rogstad and Shostak (1972) (RS); Rubin, Burbidge, and Burbidge (1964) (RBB); Rubin *et al.* (1965) (RBBCP); Rubin and Ford (RF); Shostak (1973) (S); Tully (T); and de Vaucouleurs and de Vaucouleurs (de V, de V). The radius of the easily visible disk, column (7), is based on eye estimates made by the authors. Column (8) gives the radius of the outermost H II region, which is taken from either Hodge (1967) or the furthermost H II region measured in the long-slit spectroscopic studies of these galaxies. The Holmberg radius, column (9), in kpc is either taken from the angular measurements by Holmberg (1958) or converted to his system from diameters given in the *Reference Catalogue of Bright Galaxies* through the relation given by M. S. Roberts (1969; those converted are indicated by parentheses).

Table 2 summarizes the theoretical results of the analysis described in § II as applied to 24 extragalactic systems plus our own Galaxy. Columns (2)–(4) indicate the number of components required in the mass model to fit the observed rotation curve data. Here T indicates a flat Toomre-type model and *S* refers to one or more spheroidal components. Column (5) contains the derived total mass. For several of the galaxies the rotation curve data is from 21-cm observations. Two masses are given in most of these cases: the value in parentheses represents the mass appro-

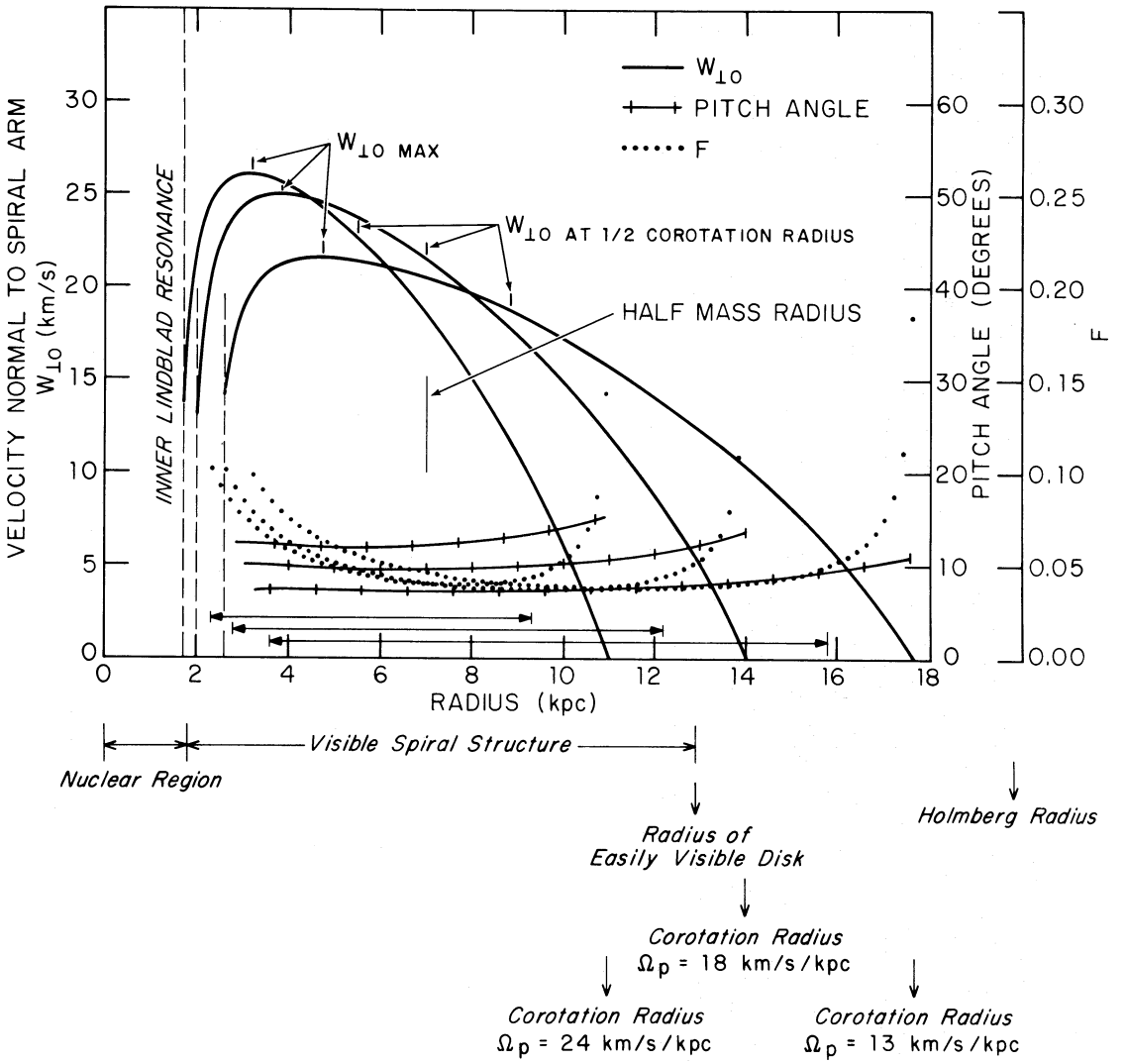

FIG. 5.—Characteristics of the density wave model of the sample galaxy NGC 224 (M31). The quantities $w_{\perp o}$, i, and F are sketched for each of three values of the pattern speed Ω_p. Although the wide range of pattern speed spanned by these values almost doubles the possible radial extent of the pattern over the disk, the levels attained by $w_{\perp o}$ are all rather similar and quite high, in the range 20–25 km s^{-1}. Since the distribution of H II regions extends well beyond everything else, corotation is thought to be more closely coincident with the radial extent of the visible spiral structure and the edge of the "easily visible" disk; and the pattern with Ω_p = 18 km s^{-1} kpc^{-1} is therefore adopted. Since $w_{\perp o}$ is so large, strong shocks are possible.

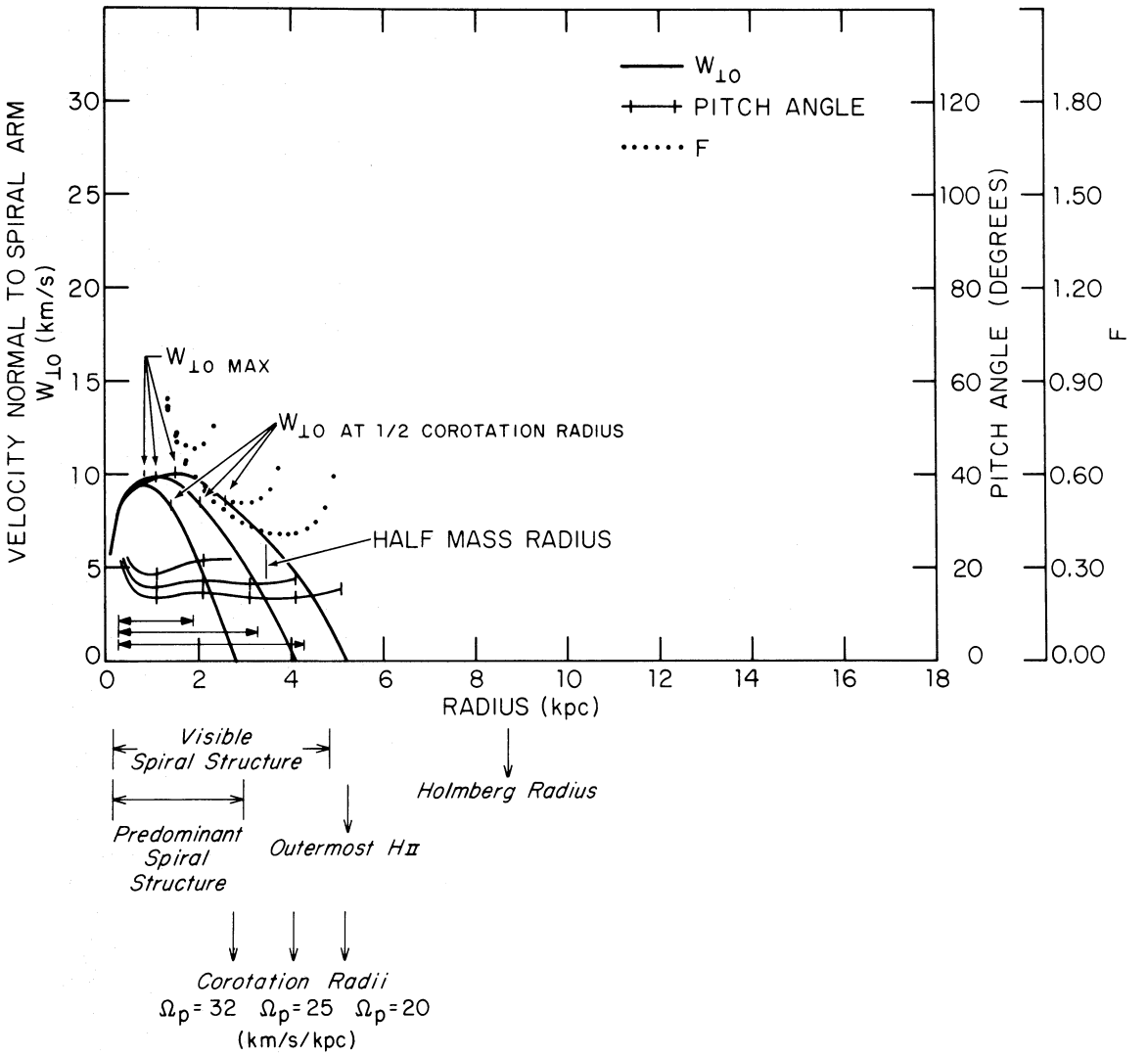

FIG. 6.—Characteristics of the density wave model of the sample galaxy NGC 598 (M33). The quantities $w_{\perp 0}$, i, and F are sketched for each of three values of Ω_p. In all three cases the levels attained by $w_{\perp 0}$ are quite low; and $w_{\perp 0}$, particularly at half corotation, remains insensitive to Ω_p. Although the distribution of H II regions and the visible spiral structure, with multiple arms in the outer parts, extend to about 5 kpc, the predominant spiral structure terminates about 2.8 kpc. For this reason the pattern with Ω_p = 32 km s^{-1} kpc^{-1} is adopted. Since $w_{\perp 0}$ is so small, only weak shocks, if any at all, are probable, and only patchy, "massive" spiral arms would be expected to be triggered.

priate to a model derived by fitting all the observed rotation curve data; the other value represents the mass appropriate to a model derived by fitting the observed rotation curve data only to a distance comparable to that covered by the optically derived data. This procedure is followed to show the uncertainty that arises from the differing observed limits in the various data available on rotation curves. For later discussion the first tabulated mass without parentheses is used. Column (6) lists the radius containing one-half the total mass. The following tabular entries relate to the application of the density wave theory. Column (7) contains the pattern speed Ω_p adopted according to the criterion for corotation discussed in § II*c*; column (8), the corresponding corotation radius ϖ_c; and column (9), the ratio of half-mass radius to corotation radius, $\varpi_{0.5M}/\varpi_c$. Column (10) gives the velocity of basic rotation relative to the pattern frame, evaluated at half-corotation, $(\Omega - \Omega_p)\varpi$. The theoretical pitch angle of the wave pattern, i, evaluated at half-corotation, is in column (11); and $w_{\perp 0}$, the velocity component of basic rotation normal to a spiral arm, also at half-corotation, is contained in column (12).

Shown in figures 5, 6, 7, and 8 are theoretical curves characterizing the density wave patterns determined for four sample galaxies: NGC 224 (M31), NGC 598 (M33); NGC 2403, and NGC 3031 (M81), respectively. The curves of $w_{\perp 0}$, i, and F are sketched for a number of possible choices of the pattern speed for each

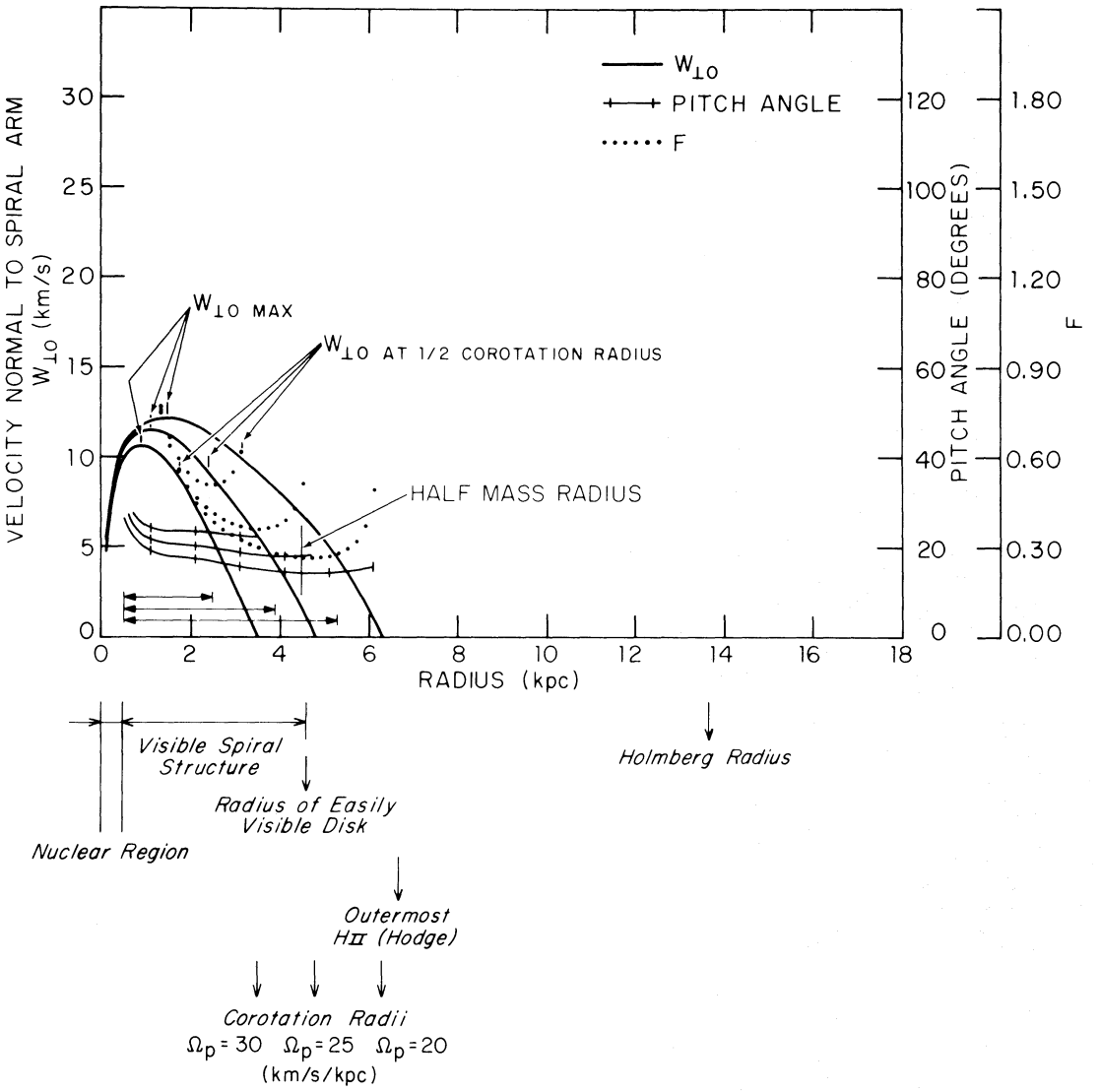

FIG. 7.—Characteristics of the density wave model for the sample galaxy NGC 2403. The quantities $w_{\perp 0}$, i, and F are sketched for each of three values of Ω_p. In all three cases the $w_{\perp 0}$ levels are low; and there is very little sensitivity of $w_{\perp 0}$ to Ω_p. In view of the radial extents of the visible spiral structure, the "easily visible" disk, and the distribution of H II regions, the pattern with Ω_p = 25 km s^{-1} kpc^{-1} appears to be a very reasonable choice; and this one is adopted. Because of the low level of $w_{\perp 0}$ here as in NGC 598 (M33), only weak shocks, if any at all, together with correspondingly patchy, "massive" spiral arms, would be probable.

galaxy. These curves for these galaxies exhibit rather well the general nature of the theoretical curves computed for all the galaxies in the sample. For example, the $w_{\perp 0}$ curves here, as for all galaxies considered, attain maxima coincident with the region of the visible spiral structure in the inner half of the disk. The superposition of three sets of curves for each galaxy illustrates that the magnitude of $w_{\perp 0}$ over its extent, and particularly at half-corotation, is very insensitive to different choices of pattern speed. The most striking case of this insensitivity is NGC 598, for which $w_{\perp 0}$ at half-corotation attains the nearly identical values of 8.3, 8.4, and 8.6 km s^{-1} although the possible choice of corotation radius is varied over a wide range. In accordance with the criterion for determining corotation discussed in § IIc, corotation is adopted at 14.0, 2.8, 4.8, and 9.7 kpc corresponding to pattern speeds of 18, 32, 25, and 26 km s^{-1} kpc^{-1} for NGC 224, NGC 598, NGC 2403, NGC 3031, respectively. In comparing these four galaxies with one another, the most striking feature of comparison is reflected in the very high levels reached by $w_{\perp 0}$ in NGC 224 and NGC 3031 and the very low levels reached in NGC 598 and NGC 2403. Consequently, strong galactic shocks are possible in NGC 224 and NGC 3031, and for this reason these galaxies are thought to be capable of exhibiting well-developed spiral structure with *narrow*, "filamentary" spiral arms. On the other hand, in NGC 598 and NGC 2403 only very weak shocks, if any at all, would be probable,

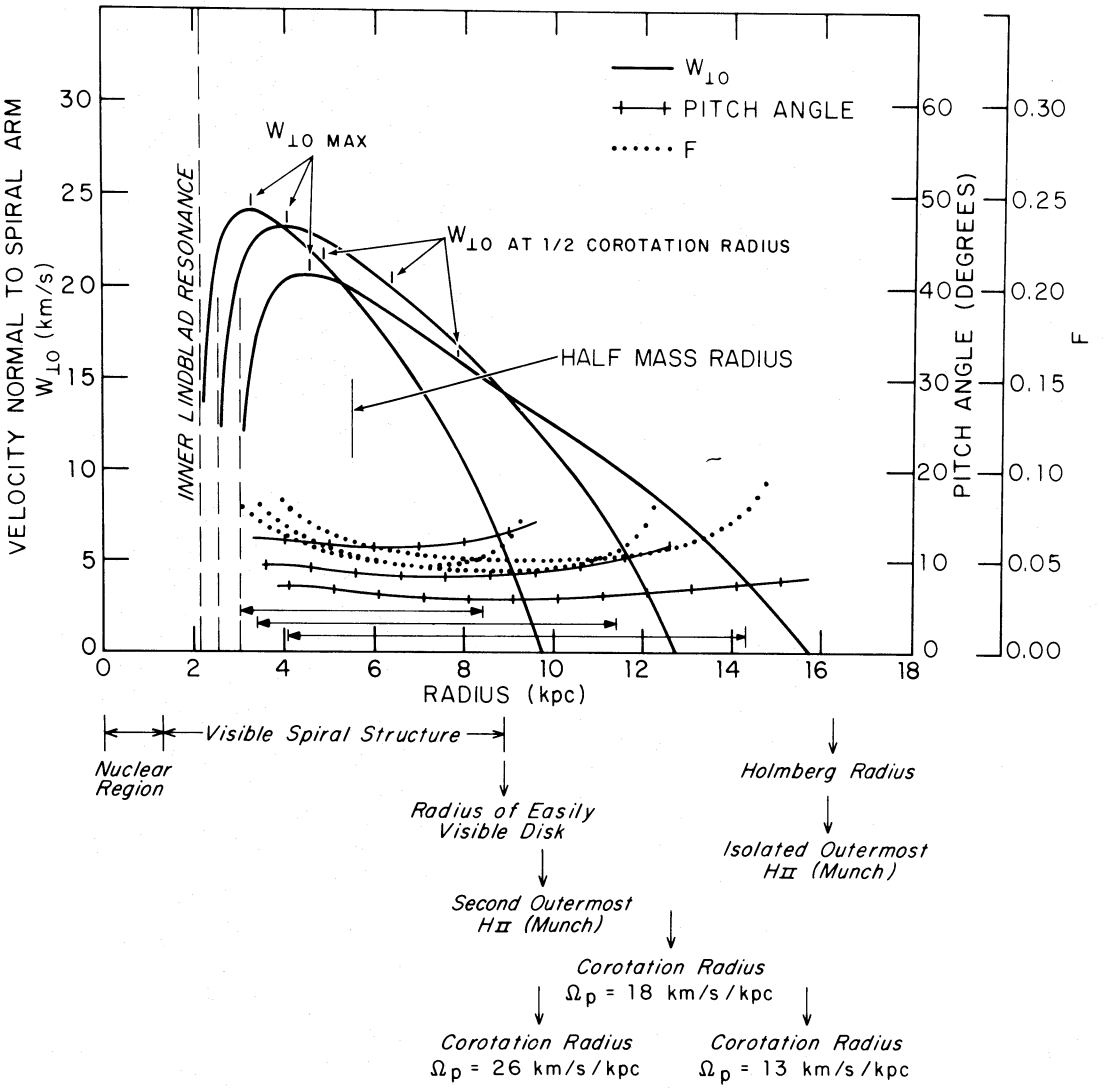

FIG. 8.—Characteristics of the density wave model for the sample galaxy NGC 3031 (M81). The quantities $w_{\perp 0}$, i, and F are sketched for each of three values of Ω_p. Here as in NGC 224 (M31), the levels attained by $w_{\perp 0}$ are quite high—in the range 20–25 km s^{-1}. The outermost H II region is an isolated one, and corotation is thought to be near the second outermost H II region which closely coincides with the radial extent of the visible spiral structure and the edge of the "easily visible" disk. The pattern with $\Omega_p = 26$ km s^{-1} kpc^{-1} is therefore adopted. Since $w_{\perp 0}$ is so large, strong shocks and correspondingly well-developed "filamentary" spiral arms are possible.

and the corresponding spiral structure would be expected to be less well developed with *broad*, "massive" arms of a more fuzzy and patchy nature.

A photograph of the sample galaxy NGC 598 (M33), with its characteristically "massive" spiral arms taken from the Hubble Atlas, is shown in figure 9. This poorly developed spiral structure with rather broad, "massive" spiral arms is thought to be a consequence of the result that only very weak shocks, if any at all, are possible in this galaxy. Superposed is the computed wave pattern. The value of 2.8 kpc for the corotation radius coincides with that estimated by Dixon (1971) through his study of the age progression of stars across the southern spiral arm of M33 for radii greater than 3 kpc. The value of 32 km s^{-1} kpc^{-1} for the corresponding pattern speed is also within the bounds determined by Courtes and Dubout-Crillon (1971) through their study of the distribution of H II regions along the same arm of M33 for radii less than 2 kpc.

Figure 10 contains a photograph of the sample galaxy, NGC 3031 (M81), with its typically "filamentary" spiral arms taken from the Hubble Atlas. This well-developed spiral structure with narrow, "filamentary" spiral arms is thought to be a consequence of the rather strong shocks possible in this galaxy. Superposed is the computed wave pattern.

These sample galaxies, M33 and M81, shown in figures 9 and 10, are two of the three galaxies considered in Shu *et al.* (1971). It is advantageous to show these here, because the computed wave patterns appear somewhat different, primarily because of the different

choices of corotation radius. The criterion for determining corotation adopted by Shu *et al.* (1971) is based solely upon the location of the outermost H II region, whereas the criterion adopted here is based upon a representative median of the radial extents of three tracers: the prominent spiral structure, the "easily visible" disk, and the distribution of H II regions. These two galaxies are prime examples of several galaxies in the sample in which the outermost patches of H II regions extend well beyond the prominent spiral structure; and it is primarily for this reason that the corotation radii adopted for M33 and M81 by Shu *et al.* (1971) are substantially greater than those adopted according to the criterion here.[7]

The theoretical wave patterns for 24 external galaxies plus our own Galaxy have been computed based upon the procedures followed and described for the sample galaxies: NGC 157 in § II; and NGC 224 (M31), NGC 598 (M33), NGC 2403, and NGC 3031 (M81) in this section. In order to compare these galaxies with each other, the fundamental parameters of total mass divided by the characteristic visible dimension of each galaxy, M/ϖ_c, and the degree of central mass concentration, $\varpi_{0.5M}/\varpi_c$, are considered together with their influence on $w_{\perp 0}$ and i. Figure 11 illustrates the $w_{\perp 0}$ surface generated by evaluating $w_{\perp 0}$ at half-corotation for the ensemble of hypothetical galaxies whose basic mass distribution is given by Toomre's model 5. The black dots indicate the locations of the 24 galaxies of the sample plus our own Galaxy with respect to this surface. All tend to lie along the general contour of the surface, although some are displaced somewhat above or below. For example, a galaxy such as NGC 224 or NGC 598, in which one or two spheroidal components are required in addition to a flat Toomre-type component, is displaced somewhat, primarily because of the additional mass of the spheroids.

The general nature of this surface is expected to be significant in determining the identity of a galaxy within the classification of galaxies. A galaxy with a mass distribution of moderate central concentration, as evidenced by the parameter $\varpi_{0.5M}/\varpi_c$ being near the value of 0.5, is found to lie near the ridge of the $w_{\perp 0}$ surface. Such a galaxy is capable of forming rather strong shock waves and is therefore predicted to have the capability of exhibiting well-developed "filamentary" spiral structure. The larger the mass of the galaxy, the higher along the ridge it can manifest itself, and the stronger the shocks to be predicted. NGC 157, NGC 224, and NGC 3031 are three prime examples where strong shocks would be predicted. On the other hand, a galaxy with a mass distribution of either very high or very low central concentration, as evidenced by the parameter $\varpi_{0.5M}/\varpi_c$ being substantially smaller or larger than 0.5, would lie along the surface at a level well below the ridge. A galaxy in this range would form only weak shocks, if any at all; and the corresponding spiral structure is expected to be less well developed and with "massive" spiral arms. Examples in which only weak shocks would be predicted are NGC 598, NGC 2403, and NGC 3109.

This $w_{\perp 0}$ surface represents an ensemble in which a value of 5 is assigned to the model number, n_T. Actually the entire sequence of values for n_T has been considered, as indicated in figure 1. Each such n_T value gives rise to a $w_{\perp 0}$ surface of the type sketched in figure 11. As n_T is assigned successive values along the sequence from large to small, the ridge of the corresponding $w_{\perp 0}$ surface shifts somewhat toward more positive $\varpi_{0.5M}/\varpi_c$. However, the overall nature of the surface and the relative locations of the galaxies lying along it remain unchanged; and for this reason the major characteristics illustrated here for $n_T = 5$ remain valid and invariant and apply over the entire sequence of n_T values (also see § VI and table 3).

V. CORRELATIONS WITH LUMINOSITY CLASS AND HUBBLE TYPE

This section investigates whether or not the concepts developed in the previous section correlate well with the observations.

a) Luminosity Class

Plotted in figure 12 along the vertical axis is the value of $w_{\perp 0}$ evaluated for each galaxy in our sample at half the radius of corotation. The galactic shock is expected to be strong in galaxies with high values of $w_{\perp 0}$ and weak in galaxies with low values of $w_{\perp 0}$. Plotted on the horizontal axis is the luminosity classification of van den Bergh (1960*a*, *b*). Figure 12 displays the predicted correlation between $w_{\perp 0}$ and the degree of development of spiral structure. Strong shocks with narrow regions of high gas compression are associated with galaxies with long, well-developed spiral arms; weak shocks with broad regions of relatively low gas compression are associated with galaxies with short, patchy spiral arms.[8]

The compressions reached in the spiral arms of 11 of the galaxies in our sample have been inferred observationally by van der Kruit (1973) from radio-continuum studies carried out using the Westerbork synthesis radio telescope. Comparison of our results with his for his subsample shows general agreement.

Strong shocks are expected not only to trigger well-developed "filamentary" arms but also to induce a high rate of star formation in a galaxy, if the gas content is sufficient; and this in turn should be reflected through a high surface brightness. This expectation seems to be consistent with the correlation found by van den Bergh between the intrinsic luminosity of a spiral galaxy and the "degree to which spiral structure is developed." Indeed, in figure 12 the galaxies with possible strong shocks are also the galaxies with high surface brightness.

[7] To be sure, the choice of corotation radius by our criterion provides a pattern speed for each of these galaxies in accord with the reasoning of Shu *et al.* (1971, p. 477): "If our determinations of the pattern speeds are to be revised at all, they should probably be revised upward."

[8] This correlation is found to be relatively insensitive to the choice of radius for evaluating $w_{\perp 0}$ in each galaxy; other radii which have been considered are quarter-corotation radius, half-mass radius, and the radius where $w_{\perp 0}$ takes on its maximum value (see, e.g., Roberts, Roberts, and Shu 1974 and Roberts 1974).

1975ApJ...196..381R

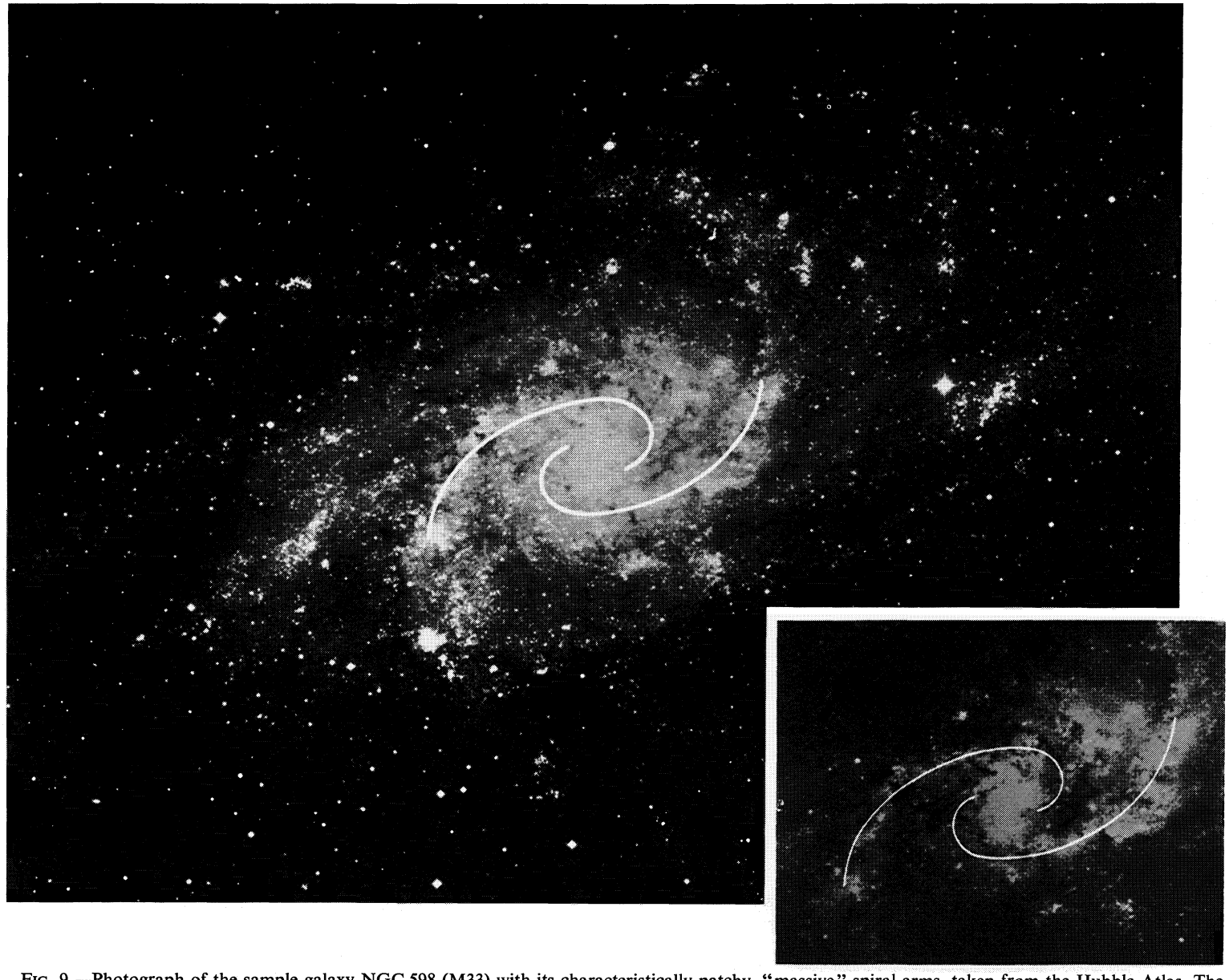

FIG. 9.—Photograph of the sample galaxy NGC 598 (M33) with its characteristically patchy, "massive" spiral arms, taken from the Hubble Atlas. The inserted photograph is one of the same scale but with less exposure. Superposed is the adopted wave pattern with $\Omega_p = 32$ km s^{-1} kpc^{-1} in which only weak shocks, if any at all, are probable. The pattern is sketched over a radial extent equivalent to its range of validity: 0.4–1.8 kpc. Corotation at 2.8 kpc therefore lies about 56% farther out in the disk from the edge of the sketch (at 1.8 kpc).